IEEE Access
Multidisciplinary ⋮ Rapid Review ⋮ Open Access Journal

Received December 15, 2020, accepted December 28, 2020, date of publication January 5, 2021, date of current version January 13, 2021.

Digital Object Identifier 10.1109/ACCESS.2021.3049223

Interpolation Accuracy of Hybrid Soft Computing Techniques in Estimating Discharge Capacity of Triangular Labyrinth Weir

ALI MAHMOUD[1], XIAOHUI YUAN[1,2], (Senior Member, IEEE), MARWAN KHEIMI[3], AND YANBIN YUAN[4]

[1]School of Civil and Hydraulic Engineering, Huazhong University of Science and Technology, Wuhan 430074, China
[2]Hubei Provincial Key Laboratory for Operation and Control of Cascaded Hydropower Station, China Three Gorges University, Yichang 443000, China
[3]Department of Civil and Environmental Engineering, Faculty of Engineering, King Abdulaziz University, Rabigh 25732, Saudi Arabia
[4]School of Resources and Environment Engineering, Wuhan University of Technology, Wuhan 430070, China

Corresponding author: Xiaohui Yuan (yxh71@163.com)

This work was supported by the National Natural Science Foundation of China under Grant 52079101.

ABSTRACT Soft Computing Techniques (SCT) are extensively used to estimate Labyrinth Weir's (LW) flow-rate. Due to the multiplicity of these techniques, identifying the most competent SCT is indispensable. This study aims to estimate the flow-rate of a sharp-crest triangular LW as a function of its side leg angle α and total head ratio (H/P) through several SCTs such as Adaptive Neuro-Fuzzy Inference System (ANFIS), Multi-Layer Perceptron (MLP), Support Vector Regression, and Radial Basis Function Neural Network. Additionally, these SCTs' potential combinations with Firefly Optimization Algorithm (FA) and Particle Swarm Optimization (PSO) are also investigated and used for estimation. The conducted experimental studies on LW examined a wide range of H/P in some limited α values. Correspondingly, all the proposed models and techniques are incapable of estimating the flow rate for intermediate α values without interpolation. Therefore, SCT's Interpolation accuracy is of the utmost importance. Besides the standard evaluation in the testing stage, a novel approach is utilized to evaluate the SCT's accuracy in the interpolation task. The SCTs are evaluated based on several statistical criteria, the Taylor diagram, Kruskal-Wallis, and Mann-Whitney tests. It is concluded that the competence of an SCT in the testing stage cannot guarantee its accuracy in the interpolation task. Subsequently, ANFIS-PSO and MLP-FA show the highest accuracy in the testing stage and interpolation task, respectively. Eventually, according to a systematic investigation in the implemented diagnostic test results, two rankings are presented for the applied SCTs based on their performance in the testing stage and their interpolation accuracy.

INDEX TERMS Triangular Labyrinth weir, soft computing techniques, interpolation accuracy, post hoc test, free-flow condition.

I. INTRODUCTION

Labyrinth Weir (LW) is a linear weir that creates a repeating pattern, i.e., cycle, by folding in plan-view. LW provides a longer crest length by its labyrinth shape, especially when there is a limitation in the channel's width. LW's increased length leads to 3-4 times higher discharge capacity of the weir compared to the straight linear weir [1]. LW reduces the upstream water level faster and more efficiently than other weir types [2]–[4]. Thus, due to LW's higher discharge efficiency, this structure can be a proper remedy for weir rehabilitation. Accordingly, LW's aptitude made this hydraulic structure a popular topic for researchers.

LW has been studied in terms of various aspects and points of view. Nonetheless, the weir's flow rate is the essential parameter [5]–[7]. Hence, the accurate estimation of LW's discharge capacity has been thoroughly investigated [8].

Due to the multiplicity of parameters affecting LW's flow rate, this value is mostly obtained experimentally. Notwithstanding, conducting an experimental study is a time-consuming and costly process. Hence, researchers had employed analytical methods to estimate the LW's flow rate.

Nonetheless, due to the complex three-dimensional flow pattern over the LW, accurate analytical solutions of head

The associate editor coordinating the review of this manuscript and approving it for publication was Gustavo Olague.

discharge relationships cannot be easily achieved [9]. Consequently, soft computing techniques could be considered as a proper alternative. The present study aims to estimate a triangular LW discharge through varieties of Soft Computing Techniques (SCT).

In 1940, Gentilini [10] conducted the first study on LW by placing multiple oblique weirs together. The LW design has been improved by other scholars that end in various forms such as triangular, trapezoidal, and rectangular. Meanwhile, LW was equipped with different crest shapes like flat, sharp, half-round, quarter-round.

Among all different forms of LW, triangular LW passes more flow than other forms [6], [11]. Thereby, researchers have conducted various experimental studies on triangular LW to elucidate this hydraulic structure behavior. In an experimental study, Ghodsian [12] confirmed the Lopes *et al.* [13] theory that the crest shape is the least affecting parameter on discharge capacity in triangular LW. Subsequently, he provided a head-discharge relationship independent of crest shape and calculated the LW's discharge coefficient (C_d) as a function of LW's total head ratio (H/P) and its effective length ratio (L/W).

Kumar *et al.* [6] studied a one-cycle sharp-crest triangular LW in the free-flow condition. They represented a regression-based equation to calculate C_d as a function of labyrinth vertex angle (θ) and H/P. Later, Bijankhah and Kouchakzadeh [7] studied a sharp-crest triangular LW in free and submerged flow conditions. They proposed a unified formula that calculates C_d in both flow conditions as a function of L/W and H/P.

According to the aforementioned experimental studies, labyrinth vertex angle (θ), total head ratio (H/P), and effective length ratio (L/W) are the most significant parameters affecting the discharge coefficient of a triangular LW. Meanwhile, the effect of flow conditions could not be neglected.

Numerous literature pieces have been published wherein SCTs have been used to estimate the C_d or Q in an LW. In 2011 Emiroglu *et al.* [14] estimated the C_d of a triangular side LW through Artificial Neural Networks (ANN). They found that ANN has higher confidence than classic models such as Multiple Non-Linear Regression (MNLR) and Multiple Linear Regression (MLR). The reported RMSE by ANN was 33.28% and 57.79% lower than MNLR and MLR, respectively. Later in 2012, Kisi *et al.* [15], in a comparison among Radial Basis Function Neural Network (RBFNN), General Regression Neural Network (GRNN), and Gene-Expression Programming (GEP), showed that RBFNN has higher confidence than other applied methods. Thereupon, Hosseini *et al.* [16], in a study on triangular LW, employed the Adaptive Neuro-Fuzzy Inference System (ANFIS) for estimating C_d as a function of the LW's side leg angle (α) and H/P. Their results confirmed the competence of ANFIS in estimating C_d.

Later, with the evolution of hybrid algorithms, in 2015, Hossein Zaji *et al.* [17] employed Particle Swarm Optimization (PSO) to improve MLR and MNLR in estimating C_d in a triangular side LW. Their results showed that the hybrid MNLR-PSO has a higher performance than RBFNN. Likewise, in another study in 2016, Zaji *et al.* [18] employed the Firefly optimization Algorithm (FA) to improve the performance of Support Vector Regression (SVR). Their results indicated that in a triangular side LW, SVR-FA can predict C_d about 10% more accurate than classic SVR.

Improvement of SVR performance by FA has also been reported in other studies. Karimi *et al.* [19] showed that SVR-FA not only has a better performance compared to the classic SVR but also is superior to the Response Surface Methodology (RSM) and Principal Component Analysis (PCA). In a study in 2020, Shafiei *et al.* [20] employed ANFIS-FA to estimate the C_d in both Triangular and Trapezoidal LW. They found that the reported results by ANFIS-FA are more accurate than a simulated LW in Computational Fluid Dynamic (CFD).

Parsaie and Haghiabi [21], through comparison of three popular ANNs (i.e., Multi-Layer Perceptron (MLP), SVR and RBFNN), found that in a triangular LW, SVR predicts C_d more accurate than MLP and RBFNN. Nevertheless, in another study on triangular LW, which was conducted by the same scholars [22], MLP not only performed better than SVR but also was superior to ANFIS, Group Method of Data Handling (GMDH), and Multivariate Adaptive Regression Splines (MARS). Likewise, Norouzi *et al.* [8] reported the superiority of MLP over SVR and RBFNN in estimating C_d in a trapezoidal LW.

Recently, Zounemat and Mahdavi [23] investigated the potential combinations of ANFIS and MLP with PSO, FA, Genetic Algorithm (GA), and Moth-Flame Optimization (MFO) in estimating the discharge capacity of the piano key weir. It is noteworthy that a piano key weir can be considered as an LW with a sloped inlet and outlet key floor. Their results revealed that the ANFIS structure performs more precise than MLP in all hybrid meta-heuristic models. Moreover, PSO improved ANFIS performance more than FA. Nevertheless, in the case of MLP, FA considerably improved MLP's performance compared to PSO, while the trained MLP with classic Levenberg-Marquardt algorithm (MLP-LM) had an acceptable performance with a shorter computational time.

The present study estimates a sharp-crest triangular LW's discharge in the free-flow condition through two empirical models and an assortment of SCTs. According to the literature review, among all the SCTs employed previously, RBFNN, MLP, ANFIS, and SVR, are the most accurate Techniques. However, the potential combination of these techniques with FA can considerably improve their accuracy. Nonetheless, in the case of ANFIS, it has been reported that its combination with PSO provides a proper technique [23], [24]. Hence, the present study aims to investigate and compare all these techniques and their hybrid version simultaneously.

It should be noted that the applied SCTs in the current study were not compared with each other previously, and to

the author's best of knowledge, no study in the published literature exploited all of them concurrently.

In the previous studies, the applied techniques have been evaluated by a random testing dataset extracted from the experimental data [14]–[23]. Consequently, this testing approach provides no clarification on the SCT's capability for estimating the intermediate values, which are not similar to either testing or training data. In order to overcome this inefficiency, the present study introduced a novel approach for assessing the SCTs interpolation accuracy.

Two sets of experimental data are adopted from the published literature [6], [7], and after generalization, they are used to train and test the SCTs. The SCTs outcomes are evaluated based on several statistical criteria, scatter plots, Taylor diagnostic test, Mann-Whitney, and Kruskal-Wallis tests.

II. MATERIALS AND METHODOLOGY

A. MATERIALS

1) EXPERIMENTAL DATASETS AND MODELS

Fig. 1 outlines a one-cycle triangular weir with a sharp crest in the free-flow condition.

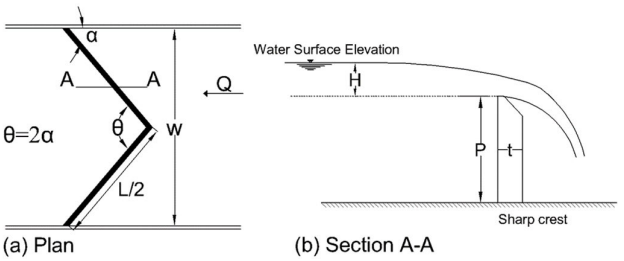

FIGURE 1. A one-cycle triangular labyrinth weir in the free-flow condition (a): plan view (b): cross-section.

Equation (1) is the general equation for the linear weirs obtained from Bazin's formula. Tullis *et al.* [1] adopted this equation for the LW study, and later, Kumar et al[6] employed it to define the head discharge relationship of triangular LW.

$$Q = \frac{2}{3} C_d L \sqrt{2g} H^{3/2} \tag{1}$$

where Q represents the weir discharge capacity, C_d denotes the dimensionless discharge coefficient, L is the total weir length, g is gravity acceleration, and H denotes the upstream piezometric head relative to weir crest elevation.

In the present study, Kumar *et al.* [6] and Bijankhah and Kouchakzadeh [7] experimental results have been exploited to train and test the SCTs. The illustrated LW in Fig. 1 is analogous to the studied LW in the adopted experimental studies [6], [7].

Kumar et al[6] carried out their experiments in a horizontal rectangular concrete channel (12 m length, 0.28 m width, and 0.41 m depth). The experiments were performed for six different weirs, which had one cycle and varieties of vertex angles ($\theta = 30°, 60°, 90°, 120°, 150$, and $180°$). Consequently, Kumar et al[6] collected 123 data and proposed (2) to calculate the C_d in triangular weir for $30° < \theta < 180°$ and $0<H/P<0.7$.

$$C_d = a_K + b_K\left(\frac{H}{P}\right) \tag{2}$$

wherein a_k and b_k are constant parameters proposed for different θ and could be found in [6].

Bijankhah and Kouchakzadeh [7] conducted their experiments in a Plexiglas flume with 12 m length, 0.6 m width, and 0.4 m depth. Their tests were performed for triangular weir in free and submerged flow conditions. In the case of the free-flow condition, four one-cycle triangular weirs with vertex angles of 74°, 90°, 120°, and 180° were examined, and 83 data were collected. Bijankhah and Kouchakzadeh [7] suggested (3) to calculate the C_d of a triangular weir in a free-flow condition and subsequently calculated the discharge capacity by (6).

$$C_d = 0.6994 \times \left[1 + \frac{a_F L^* - 1}{b_F (H/W_0)^{c_F} + 1}\right] \tag{3}$$

$$W_0 = \frac{W}{N} \tag{4}$$

$$L^* = \frac{L}{W} = \frac{1}{\sin(\alpha)} \tag{5}$$

$$Q = \frac{2}{3} C_d \sqrt{2g} w H^{3/2} \tag{6}$$

where L^* is labyrinth weir length magnification ratio, W_0 denotes the width of one cycle, a_F, b_F and c_F are constant parameters that are obtained experimentally and could be found in [7].

According to the scientific reports, in an experimental study, the effect of weir's and channel's material on LW's discharge is neglectable [1], [2]. Consequently, the described experimental datasets [6], [7] could be accumulated to provide a bigger database. However, in order to accumulate these data, performing a generalization approach is inevitable.

2) META-HEURISTIC OPTIMIZATION ALGORITHMS

a: PARTICLE SWARM OPTIMIZATION

Particle Swarm Optimization (PSO) is inspired by a bird flock's choreography and has been presented by Kennedy and Eberhart [25]. In this algorithm, particles are considered as solutions that are randomly distributed in the search space. Each particle fitness is calculated by using its position in the objective function. Moreover, a velocity vector is assigned to each particle. The velocity vector is updated in each iteration base on each particle's best personal experience (Pbest) and the best-achieved position by all particles in its vicinity (Gbest). Afterward, the new position of each particle is calculated by its velocity vector as follows [25]:

$$V_i^{it+1} = \omega V_i^{it} + \beta_1 c_1 \left(Pbest_i - X_i^{it}\right) + \beta_2 c_2 \left(Gbest_i - X_i^{it}\right) \tag{7}$$

$$X_i^{it+1} = X_i^{it} + V_i^{it+1} \tag{8}$$

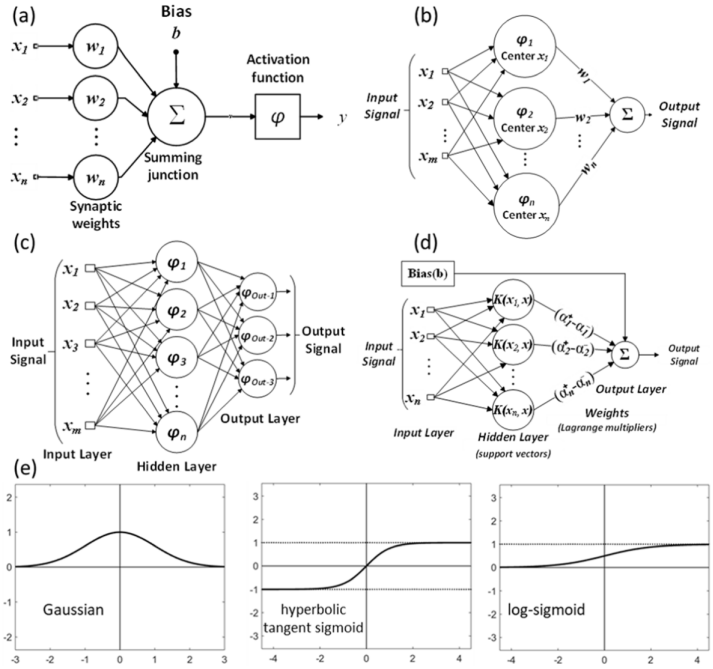

FIGURE 2. (a): A single neuron in Artificial neural networks (b): A simple radial basis function neural network (c): A multi-layer perceptron neural network (d): An architectural graph of support vector regression (e): Gaussian, hyperbolic tangent sigmoid, and log-sigmoid activation functions.

where V_i^{it+1} and V_i^{it} are velocity vector of particle i in $it+1$ and it iteration, respectively. X_i^{it+1} and X_i^{it} are particle i position in it + 1 and it iteration, respectively. $\beta 1$ and $\beta 2$ are learning factors and c_1 and c_2 are random numbers in the range [0, 1].

b: FIREFLY OPTIMIZATION ALGORITHM

Firefly Algorithm (FA) has been proposed by Yang[26]. This algorithm is inspired by Fireflies' social behavior, which are insects that produce light to attract mates and bait. Similar to other swarm algorithms, each firefly is considered as a solution. In the FA algorithm, fireflies are distributed randomly in the search space, and according to their fitness, each one has an initial brightness. The fireflies with lower brightness are attracted to the brighter fireflies. the strength of attraction between two fireflies could be calculated as follows [27]:

$$A_{i,j} = \beta_0 e^{-\gamma d_{i,j}^2} \tag{9}$$

wherein $A_{i,j}$ is the strength of attraction of firefly i towards firefly j, β_0 is the attractiveness of Ai,j at zero distance (or original light), γ is the light absorption coefficient, and it is typically between 0.001and 100, d is the distance between firefly i and j.

According to $A_{i,j}$, the new position of firefly i, which is attracted to firefly j is calculated as follows[27]:

$$x_i' = x_i + A_{i,j}\left(x_j - x_i\right) + \theta \times sgn(rand_d - \frac{1}{2})Levy_d \tag{10}$$

where x_i is the firefly i position x_i' is the new position of firefly i, x_j is the firefly j position, θ is a parameter between 0 and 1. The *randd* denotes a random vector in size of d (size of search space) whose components belong to [0, 1], Levyd is a random number drawn from Levy distribution. A detailed discussion of FA could be found in [26], [27].

3) ARTIFICIAL NEURAL NETWORK

Artificial Neural Networks (ANN) consist of plenty of simple units, namely neurons, which communicate with each other by sending information in the shape of signals. Generally, these systems adopt two different stages. In the first stage, a learning algorithm helps the system learn to perform a task, and in the next step, the system tests its computing accuracy. Several ANNs were presented using different learning algorithms, interneuron connections (structure), and activation functions. MLP, RBFNN, SVR, PCA, and many other algorithms could be classified as ANN [28]. A simple architectural graph of a single neuron in ANN is depicted in Fig. 2(a).

a: RADIAL BASIS FUNCTION NEURAL NETWORK (RBFNN)

Broomhead and lowe [29] introduced RBFNN, which has been used extensively to address regression problems [30]. RBFNN consists of three layers (i.e., input, hidden, and output). A typical RBFNN is shown in Fig. 2(b). The input layer consists of several source nodes defined by x_i to x_n, where n is the input vector's dimension. The hidden layer comprises several neurons that utilize a monotone non-increasing function as the activation function, namely, radial basis function.

The following mathematical description depicts a radial basis function [29]:

$$\varphi_i(x) = \varphi(\|x - x_i\|) \quad i = 1, 2, \ldots, n \tag{11}$$

where φ denotes a radial basis function, x_i is the center of the radial basis function, and x defines the input layer's signal. The distance which is defined by $\|x - x_i\|$ on a radial basis function plays the role of synaptic weights. Therefore, in an RBFNN, there is no weighted connection between inputs and the hidden layer. The output layer frequently leverages a linear function as the activation function. Thus, RBFNN can transform non-linear models into a linear space [28].

The present study adopts the Gaussian function in RBFNN (see Fig. 2(e)). The Euclidean distance function calculates the distance in the Gaussian function. A detailed discussion on RBFNN may be found in [28], [31], [32].

b: MULTI-LAYER PERCEPTRON (MLP)

In an MLP structure, except for the input and output layers, there are several layers of neurons called hidden layers. MLP utilizes a monotonically non-decreasing function as the activation function in the hidden layers, i.e., sigmoid function. Output neurons either leverages a sigmoid function or a linear function. Equation (12) represents the function of an MLP with one hidden layer [28].

$$Y_{net} = b_0 + \sum_{j=1}^{m} w_j \varphi\left(b_{0j} + \sum_{i=1}^{n} w_{ij} x_i\right) \tag{12}$$

where Y_{net} is the predicted value, b_0 is the bias, w denotes the weights, φ represents the activation function, x_i is the ith input, n, and m represent the number of neurons in the hidden layer and number of inputs, respectively.

In this study, the hyperbolic tangent sigmoid and log-sigmoid activation functions are used in the hidden and output layers, respectively (see Fig. 2(e)). An architectural graph of MLP with one hidden layer is shown in Fig. 2(b).

c: SUPPORT VECTOR REGRESSION (SVR)

SVR was presented by Vapnik [33] in 1995 as a supervised learning method that addresses regression problems. Employing a non-linear function (φ), SVR maps the data from a finite dimension input space (X) into a considerably higher dimensional feature space (F) to constructs a linear model in feature space. By this means, the SVR output based on Vapnik theory can be expressed by the following equation:

$$f(x) = w\varphi(x) + b \tag{13}$$

where w is a normal vector, φ(x) is the multi-dimensional space feature that maps the input space vector x to F, b is a scalar. Unlike MLP and RBFNN, the SVR training process is not based on minimizing the difference between target and output values (i.e., error); instead, SVR minimizes the empirical risk in its training process. For a dataset with n samples, each sample can be discriminated as: $\{x_i, d_i\}_i^n$, where x_i and d_i are input and target vector, respectively. Thus, the SVR training objective function can be expressed by *(14)*.

$$R_{SVM}(C) = \frac{1}{2}\|w\|^2 + C\frac{1}{n}\sum_{i=1}^{n} L(x_i, d_i) \tag{14}$$

where $\frac{1}{2}\|w\|^2$ is the regularization term, $C\frac{1}{n}\sum_{i=1}^{n} L(x_i, d_i)$ represents the empirical risk function, C is the error penalty factor, and $L(x_i, d_i)$ is the loss function which determines the accuracy of training data point based on an allowed value (ε) and slack variables (ξ_i^+ and ξ_i^-) that determine the lower and upper excess deviation. By minimizing the *(14)* w and b are obtained as follow:

$$\min R(w, \xi_i) = \frac{1}{2}\|w\|^2 + C\sum_{i=1}^{n}(\xi_i^+ + \xi_i^-)$$
$$subject\ to \begin{cases} d_i - w\varphi(x_i) + b_i \le \varepsilon + \xi_i^+ \\ w\varphi(x_i) + b_i - d_i \le \varepsilon + \xi_i^- \\ \xi_i^+, \xi_i^- \ge 0 \quad i = 1, 2, \ldots, l \end{cases} \tag{15}$$

Eventually, concerning (15) and employing the kernel trick and Lagrange multiplier and optimality constraints, (13) can be represented as follow:

$$f\left(x, \alpha_i^+ \alpha_i^-\right) = \sum_{i=1}^{n}(\alpha_i^+ - \alpha_i^-)K\left(x_i, x_j\right) + b \tag{16}$$

where $K(x, x_i)$ is the kernel function, which is the product of the two inner vectors x_i and x_j. in the feature space $\varphi(x_i)$ and $\varphi(x_j)$. α_i^+ and α_i^- are Lagrange values determined by ξ_i^+ and ξ_i^-. Verities of kernel functions are introduced in SVR; nonetheless, linear, polynomial, RBF, and Sigmoid kernel functions are more prevalent in solving general problems [21], [22]. Among the mentioned kernel functions, RBF, due to its higher efficiency, is more accomplished in complex problems [18], [34]; thus, the present study employs the RBF kernel function in SVR. An architectural graph of SVR is shown in Fig. 2(d).

4) ADAPTIVE NEURO-FUZZY INFERENCE SYSTEM (ANFIS)

ANFIS is a combination of the Fuzzy inference system (FIS) and ANN, which can model complex systems based on input and output data [35]. In a fuzzy system with two inputs and rules, the fuzzy rules can be expressed as:

$$\text{Rule 1}: \textit{if } x \textit{ is } A_1 \textit{ and } y \textit{ is } B_1 \textit{ then } f_1 = p_1 x + q_1 y + b_1 \tag{17}$$

$$\text{Rule 2}: \textit{if } x \textit{ is } A_2 \textit{ and } y \textit{ is } B_2 \textit{ then } f_2 = p_2 x + q_2 y + b_2 \tag{18}$$

wherein A_1, A_2, and B_1, B_2 are Membership Functions (MF) for input x and y, respectively. f_1 and f_2 are output functions; p, q, b are the parameters of output functions. For more simplicity, these rules are shown in Fig. 3(a).

ANFIS structure consists of five layers. This structure for an ANFIS with two inputs is illustrated in Fig. 3(b). It should be noted that for more simplicity, the following equations concerning ANFIS functioning are presented for an ANFIS with two inputs. In the first layer, input nodes are entered, and

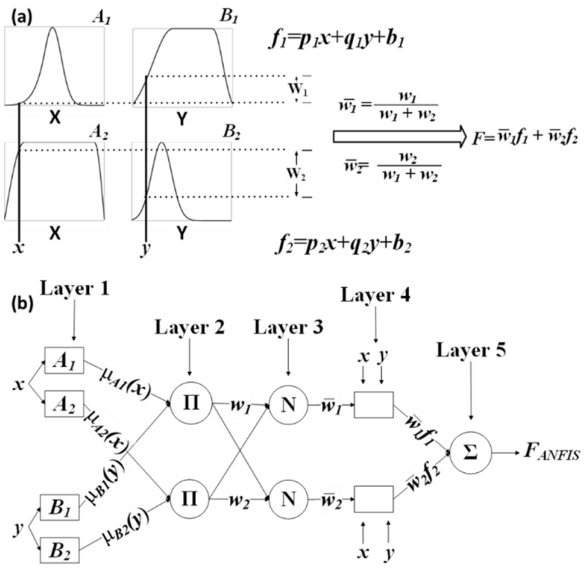

FIGURE 3. (a): Illustration of inputs and outputs membership function in ANFIS (b): ANFIS structure.

MFs are assigned to them ((17) and (18)). The second layer determines the weight (w_i) of rules by a T-norm as follows:

$$w_i = \mu_{A_i}(x) \times \mu_{B_i}(y) \quad i = 1, 2 \tag{19}$$

where, $\mu_{A_i}(x)$ and $\mu_{B_i}(y)$ are values of MFs (A_i and B_i) for inputs x and y. The third layer normalizes the determined weight of the rules as follows:

$$\bar{w}_i = \frac{w_i}{\sum_i w_i} \quad i = 1, 2 \tag{20}$$

where $\bar{w}_i$ is the normalized weight of input i. The fourth layer computes the contribution of the entire rule as:

$$F_i = \bar{w}_i f_i \quad i = 1, 2 \tag{21}$$

where F_i represents the output for input i. Eventually, the final layer summarizes the outputs and gives the network output as follows:

$$F_{ANFIS} = \sum_i F_i \quad i = 1, 2 \tag{22}$$

According to (19)-(22), and Fig. 3, it is abundantly clear that applying some modifications on MFs leads ANFIS to approach different outputs. Considering a target output, the difference between ANFIS's output and the defined target can represent the error. Afterward, the ANFIS structure can be trained by an optimization algorithm that modifies MF's parameters to minimize the error. In machine learning approaches, this algorithm is called the learning algorithm or training algorithm.

It should be noted that the present study utilizes the Subtractive Clustering Method (SCM) to generate the initial ANFIS structure (MFs, fuzzy rules, MF's dimensions, and their locations). SCM was introduced by Chiu [36]. In this method, by considering each data point as a candidate for a cluster center, each data density is measured according to the number of other data in its vicinity. Thereafter, the data with the highest density are chosen as the cluster's center, and the density of other data are revised based on it. This loop is repeated until a sufficient number of clusters is generated. The detailed explanations about SCM can be found in [36] and MATLAB's help.

By employing SCM, MATLAB return a complete FIS according to the input and target data. Subsequently, considering these parameters as a decision variable vector, any classic or meta-heuristic optimization algorithm could be employed to train ANFIS.

5) EVALUATION METRICS

a: STATISTICAL CRITERIA

In order to evaluate the performance of the employed SCTs, their outcomes are evaluated in terms of the Pearson's linear correlation coefficient (R), Mean Absolute Error (MAE), Root Mean Square Error (RMSE), Nash-Sutcliffe (NSE), the index of agreement (IA) and Mean Absolute Percentage Error (MAPE). The following equations calculate these metrics:

$$R = \frac{\sum_{i=1}^{N}(T_i - \bar{T})(O_i - \bar{O})}{\sqrt{\sum_{i=1}^{N}(T_i - \bar{T})^2 \sum_{i=1}^{N}(O_i - \bar{O})^2}} \tag{23}$$

$$MAE = \frac{1}{N}\sum_{i=1}^{N}(|T_i - O_i|) \tag{24}$$

$$RMSE = \sqrt{\frac{1}{N}\sum_{i=1}^{N}(T_i - O_i)^2} \tag{25}$$

$$NSE = 1 - \frac{\sum_{i=1}^{N}(T_i - O_i)^2}{\sum_{i=1}^{N}(O_i - \bar{O})^2} \tag{26}$$

$$IA = 1 - \frac{\sum_{i=1}^{N}(T_i - O_i)^2}{\sum_{i=1}^{N}\left(|T_i - \bar{O}| + |O_i - \bar{O}|\right)^2} \tag{27}$$

$$MAPE = \frac{1}{N}\sum_{i=1}^{N}\frac{|T_i - O_i|}{T_i} \times 100 \tag{28}$$

$$RMSD = \sqrt{\frac{\sum_{i=1}^{N}\left((O_i - \bar{O}) - (T_i - \bar{T})\right)^2}{N}} \tag{29}$$

where N denotes the number of variables, T_i is the ith target value, $\bar{T}$ is the mean of target values, O_i represents the ith output value, $\bar{O}$ denotes the mean of output values. It is noteworthy that $(T_i - O_i)$ denotes the error.

b: TAYLOR DIAGRAM

Taylor [37] proposed a single diagram to visualize how closely a model predicts the observed values based on its Root Mean Square Difference (RMSD), Correlation Coefficient (R), and Standard Deviation (STD). The Taylor diagram specifies models as a series of points on a polar plot. The azimuth angle of the diagram shows the R between the observed and predicted datasets. The R between the observed dataset and itself is equivalent to one; therefore, the reference point (observed dataset) locates on the line with an azimuth

angle equal to 0°. Furthermore, the normalized STD of the observed dataset determines its distance from the center of the polar plot. The same procedure is repeated for all predicted datasets, while the radial distance from the reference point represents the RMSD (29). In this manner, the location of predicted datasets and their distance from the reference point designates their similarity to the observed dataset.

c: KRUSKAL-WALLIS TEST

Kruskal-Wallis test [38] is a nonparametric test used to investigate whether there is a significant difference between several groups, or all the groups originated from the same distribution. The superiority of the Kruskal-Wallis test over the Mann-Whitney test is in its capability to investigate more than two datasets simultaneously. The null hypothesis of the Kruskal-Wallis test is that the mean rank of all groups is equal. Nonetheless, by rejecting the null hypothesis, the Kruskal-Wallis test cannot distinguish the different groups. Therefore, in this study, a "post hoc" test is applied to specify the probable groups which are different from the observed dataset. Moreover, the Mann-Whitney test is applied to investigate the significant difference between the estimated values through each SCT and the observed values.

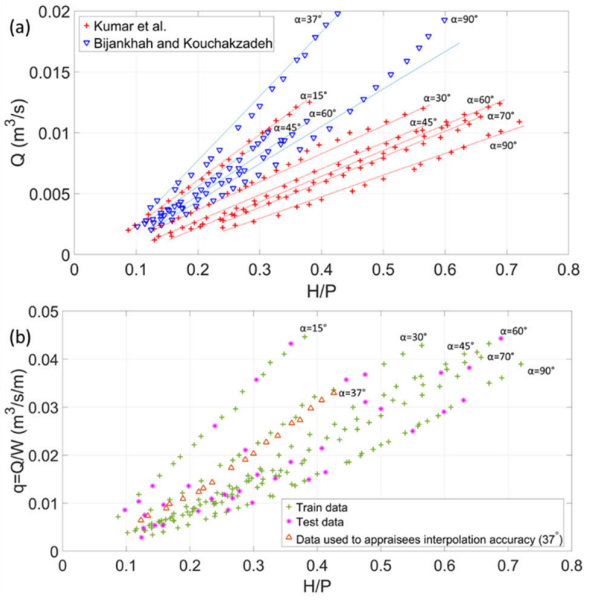

FIGURE 4. (a): Q versus H/P in the obtained experimental datasets, without generalization (b): the discharge per-unit-width (q) versus H/P in the generalized database and the split of data for training, testing, and appraising interpolation accuracy in the current study.

B. METHOD

the present study utilizes SCT to estimate a triangular LW discharge capacity according to two sets of experimental results [6], [7]. The observed discharge capacities versus H/P in these experiments for different α are illustrated in Fig. 4(a). According to Fig. 1 and (1), the labyrinth length (L) decreases with an increase in α. Consequently, greater α results in a smaller discharge capacity. Hence, the illustrated data in Fig. 4 (a) do not follow a logical sequence and need to be generalized. The adopted experimental studies were conducted in two rectangular channels with different widths. To eliminate the effect of channel width and subsequently generalize the experimental results, the present study considered discharge per unit width (q) as the estimation target. Fig. 4(b) demonstrates the generalized experimental data. The logical sequence of data based on their α is abundantly clear in Fig. 4(b).

According to (1), the discharge capacity of an LW is a function of C_d, L, H, and g. Likewise, the experimental studies proved that the C_d is a function of H/P, L/W, and θ. Considering q as the estimation target, the W is eliminated from the calculations. According to the fact that L is equivalent to $1/\sin(\alpha)$ in an LW with unit width, the q could be estimated by (30).

$$q = f\left(\frac{H}{P}, \frac{1}{\sin(\alpha)}\right) \tag{30}$$

Similar to the obtained experimental study in this research, all the conducted experimental studies on LW examined a wide range of H/P in some limited α values. As an example, Kumar *et al.* [6] investigated six different α values. They proposed an empirical model for these six angles, while in a real-world problem such as Ute dam's LW, the LW is designed with an intermediate α (33.9°) [39]. Furthermore, in a continuous space like the LW optimization problem [16], α could take any intermediate value. Thus, in a real-world problem, the α is not precisely equal to the experimented values. Accordingly, the SCT's confidence in estimating the LW's flow rate for intermediate α angles is of the utmost importance.

Concerning the importance of SCT's interpolation accuracy, it should be noted that the previous studies evaluated their techniques with a testing dataset extracted randomly from the experimental data. Although this approach is the standard approach for evaluating the SCT's accuracy, it cannot clarify the SCT's accuracy in the interpolation task. Therefore, in order to identify the most competent SCT for estimating LW's discharge, it is necessary to evaluate the SCT's interpolation accuracy.

For Appraising the accuracy of applied SCTs in the interpolation task, one set of data with an intermediate α is not used for either training or testing. The present study considered the LW with α equals to 37° for appraising interpolation accuracy. Afterward, the SCTs which are trained with six different α (i.e., 15°, 30°,45°,60°,75°, and 90°) are used to estimate the discharge capacity in LW with α equals to 37°. Comparing estimated and observed q in LW with α equals 37° appraises the SCTs competence in the interpolation task. The split of data for training, testing, and appraising interpolation accuracy is illustrated in Fig. 4(b).

Due to the multiplicity of the classic and hybrid SCTs used in estimating LW's flow rate, it is not practicable to evaluate all of them in one research. However, there is no doubt that identifying the most competent SCT is indispensable. The

present study identified the most competent SCTs in previous researches and investigated their capability in the regular tasting stage and interpolation tasks.

Reviewing the published literature (2010-2020) indicates that among all the applied SCTs, MLP, ANFIS, SVR, and RBFNN are the most accurate Techniques.

Furthermore, with the evolution of hybrid techniques, researchers employed meta-heuristic algorithms for training the SCTs. According to the literature review, among all the meta-heuristic algorithms employed for training SCTs, FA is one of the most qualified algorithms. However, in the case of ANFIS, it has been reported that PSO has higher efficiency than FA. Thus, in addition to the classic SCTs mentioned above, the present study investigates four hybrid SCTs, including ANFIS-PSO, ANFIS-FA, SVR-FA, and MLP-FA.

In the present study, the standard version of ANFIS is trained by hybrid Back Propagation, and Least mean Square (BP&LS). This prevalent algorithm is exploited in MATLAB, and its detailed explanation can be easily found in literature and the MATLAB's help. In addition to BP&LS, FA and PSO are also employed to train the ANFIS. In both ANFIS-FA and ANFIS-PSO, the MF's parameters (see Fig. 3) play the role of decision variables while FA and PSO minimize the RMSE between targets and outputs. According to Fig. 3, in the defined Sugeno FIS, the output functions are linear, and each one is defined by three parameters (i.e., p, q, r). The input MFs are Gaussian, and each one is defined by two parameters that identify the mean (c) and variance (σ) of the Gaussian MF. Compared to other membership functions such as trapezoidal, triangular, and sigmoid, the Gaussian membership function, due to its smoothness, increases the FIS's flexibility and accuracy in C_d estimation [40]. Algorithm 1 shows the pseudo-code for training ANFIS with a meta-heuristic algorithm (PSO and FA in the current study).

The standard version of MLP with one hidden layer consist of 15 neurons is trained with the classic Levenberg-Marquardt algorithm. Thus, this ANN is mentioned as MLP-LM. The hybrid version of MLP (MLP-FA) inherits the same structure, activation functions, number of layers, and neurons from MLP-LM. In the training procedure, FA takes the b_0 and w from each neuron (see (12)) as decision variables and minimizes the Root Mean Square Error (RMSE) between targets and outputs.

In the case of RBFNN, the present study calculates the number of neurons by the following equation. [41].

$$H_n = \frac{M+N}{2}\sqrt{T_n} \tag{31}$$

wherein H_n is the number of neurons in the hidden layers, M and N denote the input and output size, respectively, and T_n is the training dataset's size. In this study, RBFNN has trained with the Gradient Descent algorithm (GD) proposed in MATLAB.

The standard version of SVR is trained with the classic Interior Point Method (IPM), and in the hybrid version (SVR-FA), the FA is exploited to train SVR with minimizing the empirical risk (see (15)).

In order to provide a better perspective on the evaluation procedure, Fig. 5 is provided to show the methodology of the current study.

Algorithm 1 Pseudo-Code of Training ANFIS With a Meta-Heuristic Algorithm

1. *Define the input and targets*
   inputs = (H/P, 1/sin(α)), target = observed-q
2. *Generate the initial FIS with SCM*
3. *Start the meta-heuristic algorithm*
   Define the initial parameters
   Define the maximum number of iterations (it_{max})
   It = 0
4. ***While****it<it max*
5. *Extract the FIS parameters and define them as a decision variables vector (p_i, q_i, r_i, σ_i, c_i) i = 1, 2, 3, . . ., m = number of inputs*
6. *Calculate the FIS output (Train-output) using the input data (in MATLAB, calculate by "evalfis (FIS, inputs)")*
7. *Calculate the RMSE between Train-output and observed-q (meta-heuristic algorithm's objective)*
8. *Apply modification on the decision variable vector according to the employed meta-heuristic algorithm*
9. *Allocate the decision variables (FIS's parameters) to their specific place on FIS*
10. *It = it+1*
11. ***End while***
12. *Report the final FIS*

III. RESULTS AND DISCUSSION

In common with other machine learning approaches, the obtained database is divided into training and testing sets. In the current study, two experimental datasets [6], [7] are generalized and combined, which provides 206 data. As illustrated in Fig. 4 (b), 18 data (8.7% of all data) associated with LW with α =37° were taken out from the training and testing datasets and further used to assess the SCT's interpolation accuracy. Thereby 188 data remained for training and testing stages. It should be noted that data split ratios intensively affect the SCT's performance. Allocating a big percentage of the database for the training increases the overfitting chance. On the contrary, using a small training dataset and a big testing dataset causes underfitting.

Several trials with different training percentages, such as 80%, 70%, 65%, and 60%, are conducted to determine the best data split for training and testing stages. Consequently, allocating 80% of the database (151 data) for training and 20% (37 data) for testing submitted the best performance. The conducted test and error trial indicates that both underfitting and overfitting decrease the SCT's accuracy in the interpolation task. In comparison, the destructive effect of over-fitting

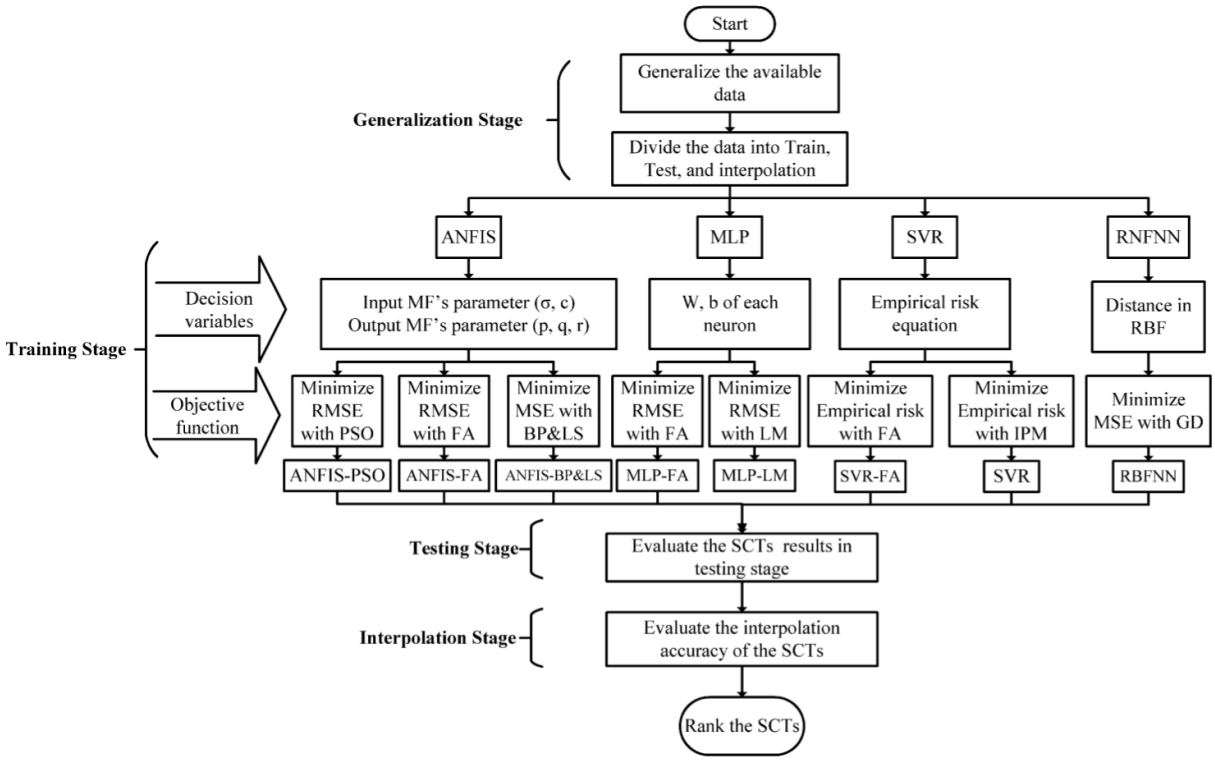

FIGURE 5. Methodology flowchart.

on interpolation is more severe. It should be noted that the same database and split of data (for training and testing) is used for all SCTs (see Fig. 4).

The initial parameters of PSO and FA highly affect the optimization results, which are inextricably connected to the problem characteristic (e.g., number of decision variables, the size of decision variables vector, objective function's dimension, and size of search space) [27]. Therefore, the optimal value of these parameters is mostly obtained by several trials with giving different parameters range. In the current research, in all hybrid SCTs, FA is executed with the light absorption coefficient (Υ) and Original light (β_0) equivalent to 2 and 1, respectively. Likewise, the Personal learning factor (β_1) and Global learning factor (β_2) in PSO are considered 1 and 2, respectively. Moreover, in both PSO and FA, the swarm size is equivalent to 50.

In addition to the applied SCTs, two empirical models proposed by Kumar *et al.* [6] and Bijankhah and Kouchakzadeh [7] are also used for estimation. Due to the incapability of these models ((2),(3)) in estimating intermediate values, they are compared with SCTs in the testing stage. The statistical criteria evaluation on training, testing, and interpolation stage after 2000 epochs is tabulated in Table 1. Moreover, the same results in the testing stage and interpolation task are illustrated in Fig. 6.

The reported results in Table 1 imply that SCTs are performed better than empirical models. The average R, IA, and NSE for all SCTs in the testing stage are 3.38%, 2.64%, and 10.75% higher than the average values for empirical models, respectively. Likewise, the average MAPE for all SCTs is 6.42% lower than the empirical models' average MAPE.

According to the reported results in Table 1, it is evident that employing meta-heuristic algorithms for training SCTs has improved their estimation accuracy, which is in agreement with previously published results [18]–[20], [23]

In the case of ANFIS structure, ANFIS-FA has the best performance in the training stage, and ANFIS-PSO reports better performance in the testing stage, while in both training and testing stages, ANFIS-PSO and ANFIS-FA estimated q with higher confidence than ANFIS-BP&LS. Nevertheless, regardless of the employed training algorithm, the ANFIS structure reports a feeble performance in the interpolation task. However, it seems that using meta-heuristic algorithms for training ANFIS improves its accuracy in the interpolation task, when ANFIS-PSO and ANFIS-FA estimate the q with 39.34% and 30.39% lower MAPE than ANFIS-BP&LS, respectively.

In MLP, employing FA instead of LM improves the MLP performance in the testing stage, when MLP-FA reports 0.0367 ltr/s/m and 0.0157 ltr/s/m lower RMSE and MAE than MLP-LM, respectively. Likewise, in the interpolation task, MLP-FA not only reports 3.162 ltr/s/m, 3.06 ltr/s/m, and 17.31% lower RMSE, MAE, and MAPE than MLP-LM but also submits the best fit among all the applied SCTs.

TABLE 1. Performance evaluation of the applied SCTs for estimating LW's discharge in the training stage, testing stage, and interpolation task.

Stage	SCT	statistical criteria					
		R	IA	NSE	RMSE*	MAE*	MAEP
train	ANFIS-BP&LS	0.9995	0.9997	0.999	0.3573	0.2574	1.579
	ANFIS-FA	**0.9998**	**0.9999**	**0.9996**	**0.2087**	**0.1334**	**0.82**
	ANFIS-PSO	0.9997	0.9998	0.9994	0.2764	0.1988	1.202
	MLP-LM	0.9996	0.9998	0.9992	0.3146	0.2312	1.454
	MLP-FA	0.9996	0.9998	0.9992	0.3133	0.2232	1.474
	SVR	0.9993	0.9996	0.9986	0.416	0.343	2.451
	SVR-FA	0.9996	0.9998	0.9993	0.2806	0.1827	1.149
	RBFNN	0.9989	0.9994	0.9978	0.5247	0.3993	2.585
test	ANFIS-BP&LS	0.9993	0.9996	0.9985	0.4534	0.3517	2.39
	ANFIS-FA	0.9994	0.9996	0.9987	0.3757	0.3056	2.131
	ANFIS-PSO	**0.9996**	**0.9997**	**0.9998**	**0.374**	**0.288**	**2.103**
	MLP-LM	0.9994	0.9996	0.9986	0.444	0.3455	2.455
	MLP-FA	0.9995	0.9997	0.9988	0.4073	0.3298	2.424
	SVR	0.9961	0.9996	0.9984	0.4733	0.3936	2.946
	SVR-FA	0.9977	0.9997	0.9988	0.4061	0.305	2.322
	RBFNN	0.9967	0.9994	0.9978	0.5577	0.4588	3.239
	Kumar et al. [6]	0.9572	0.9665	0.8739	1.1	0.6912	10.24
	Bijankhah [7]	0.976	0.9812	0.9294	0.8383	0.5168	7.604
interpolation	ANFIS-BP&LS	0.9989	0.8427	0.1344	7.8404	7.7526	49.872
	ANFIS-FA	0.9849	0.9565	0.7557	4.1648	3.4227	19.484
	ANFIS-PSO	0.9913	0.9916	0.9623	1.6349	1.4927	10.533
	MLP-LM	0.9962	0.9495	0.8081	3.6911	3.521	20.595
	MLP-FA	**0.9984**	**0.9989**	**0.996**	**0.529**	**0.4611**	**3.284**
	SVR	0.9965	0.9969	0.9876	0.9379	0.8109	5.324
	SVR-FA	0.9982	0.9975	0.9896	0.8553	0.7681	4.657
	RBFNN	0.9986	0.9986	0.9945	0.6212	0.5444	4.093

* ltr/s/m

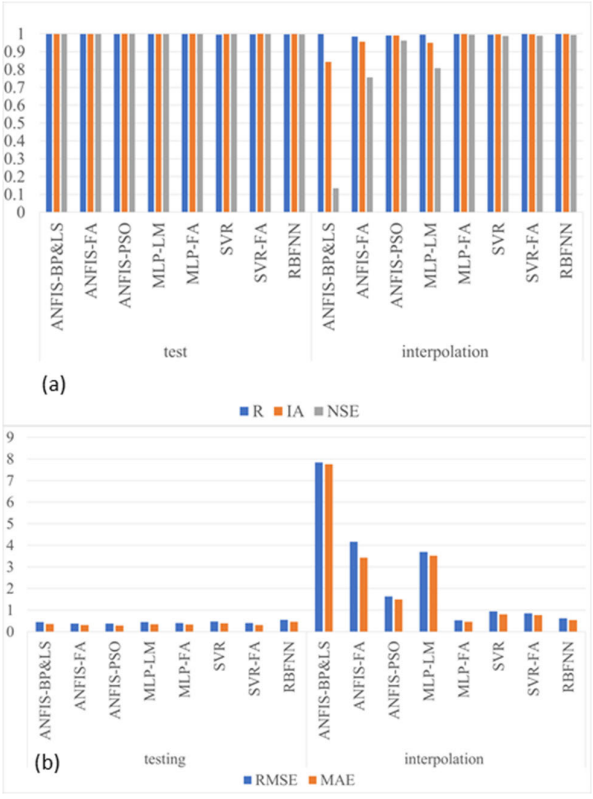

FIGURE 6. The graphical illustration of statistical criteria in the testing stage and the interpolation task (a): R, IA, NSE (b): RMSE, MAE.

Similar to MLP, the SVR performance is also improved by exploiting FA. SVR-FA reports 1.3%, 0.62%, and 0.67% lower MAEP than classic SVR in training, testing, and interpolation stages, respectively. Regardless of the adopted training algorithm, SVR shows an acceptable performance in all three stages, while this behavior is not observed in ANFISs and MLP.

The performance of RBFNN in the training and testing stages is inferior to the performance of all the other applied SCTs. In comparison to the average MAPE for all the applied SCTs, RBFNN reports 1% and 0.74% higher MAPE in the training and testing stages, respectively. Nonetheless, in the interpolation task, RBFNN estimates the q with great confidence when the reported MAPE buy RBFNN is just 0.8% higher than MLP-FA.

Taking into account that all the previous studies evaluate their applied SCTs with a random testing dataset (similar to the test stage in Table 1), and without considering the interpolation accuracy, it can be argued that the ANFIS-PSO has the highest accuracy among all the applied SCTs.

Table 2 compares the statistical criteria of ANFIS-PSO with the most accurate SCTs that have been reported in the previous studies on triangular LW. Accordingly, ANFIS-PSO outperforms other compared SCTs in the standard testing approach. Notwithstanding, the current study's main hypothesis is that an SCT's performance in a random testing dataset cannot guarantee its accuracy in estimating intermediate data.

In order to prove the described hypothesis, the SCTs' performance in the testing stage and interpolation task is extensively investigated.

The results of each employed SCTs in the form of scatter plots for testing and interpolation stages are illustrated

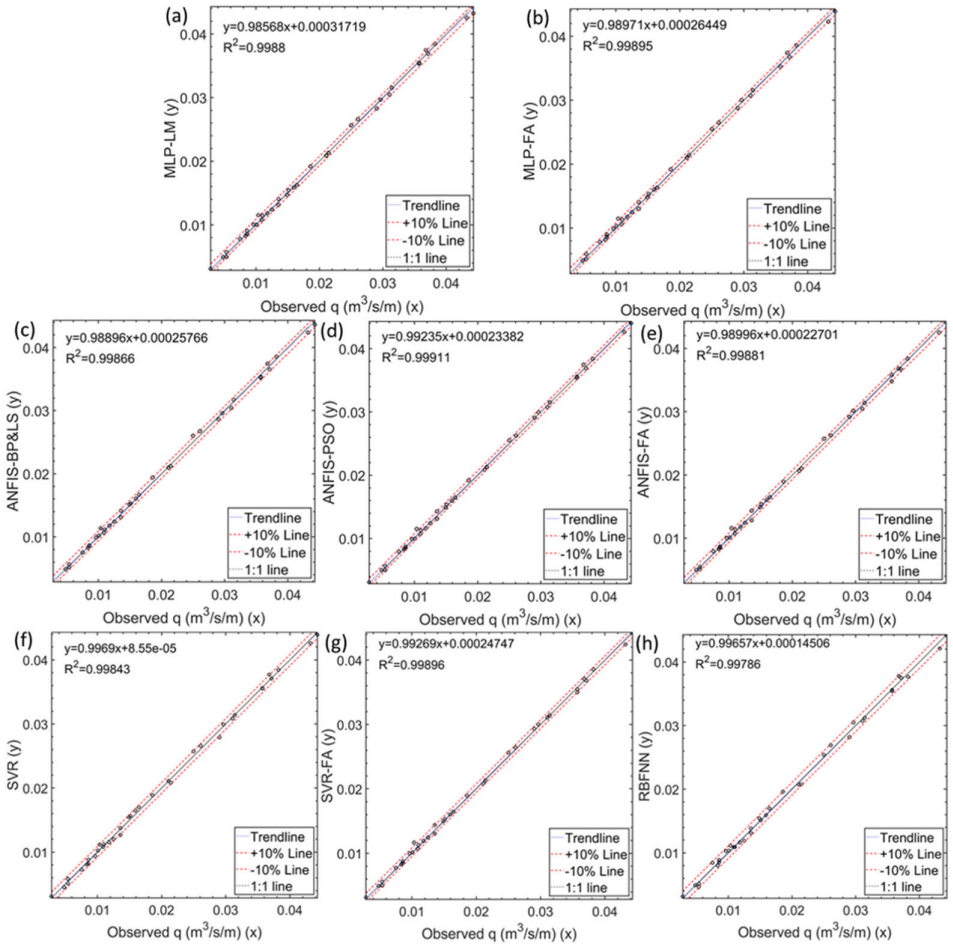

FIGURE 7. Scatter plot for observed q versus estimated q in the testing stage through (a): MLP-LM (b): MLP-FA (c): ANFIS-BP&LS (d): ANFIS-PSO (e): ANFIS-FA (f): SVR (g): SVR-FA (h): RBFNN.

TABLE 2. Comparison of the most accurate SCT in the current study and previous studies according to the standard testing approach (random testing dataset).

authors	LW configuration	Best SCT	Statistical criteria					
			R	IA	NSE	RMSE	MAE	MAEP
Emiroglu et al. [14]	Triangular side LW	ANN	0.978	✗	✗	0.0674	0.0434	✗
Kisi et al. [15]	Triangular side LW	RBFNN	0.979	✗	✗	0.067	0.043	✗
Hosseini et al. [16]	Triangular LW	ANFIS	0.9988	✗	✗	0.0027	0.00186	✗
Zaji et al. [17]	Triangular LW	MNLPSO	0.942	✗	✗	0.0223	0.0186	2.8577
Zaji et al. [18]	Triangular side LW	SVR-FA	0.9413	✗	✗	0.035	0.026	4.088
Karimi et al. [19]	Triangular LW	SVR-FA	0.9899	✗	✗	0.005	0.003	8
Parsaie and Haghiabi [22]	Triangular LW	SVR	0.9695	✗	✗	0.038	✗	✗
Parsaie and Haghiabi [23]	Triangular side LW	MLP	0.9798	✗	✗	0.07	✗	✗
The current study	Triangular LW	ANFIS-PSO	0.9996	0.9997	0.9998	0.003	0.0029	2.103

in Figs. 7 and 8, respectively. Visual investigation of the scatter plots in Fig. 7 reveals that the distributed points associated with all the SCTs are significantly close to the line of agreement. Thus, it can be argued that in the testing stage, all the applied SCTs are estimating q with great confidence. Moreover, the +10% and −10% Confidence Interval (CI) lines in all the ANFISs and MLP-FA are considerably closer to the defined trendline, which expresses these models' high accuracy in harmony with the proposed results in Table 1. It should be reminded that the tested data are randomly chosen from the training dataset and subsequently are similar to them.

As depicted in Figs. 8(a) and 8(c), the distributed points associated with MLP-LM and ANFIS- BP&LS are not close to the line of agreement. Thereby, despite their high correlation coefficients, these two SCTs submit the highest error in

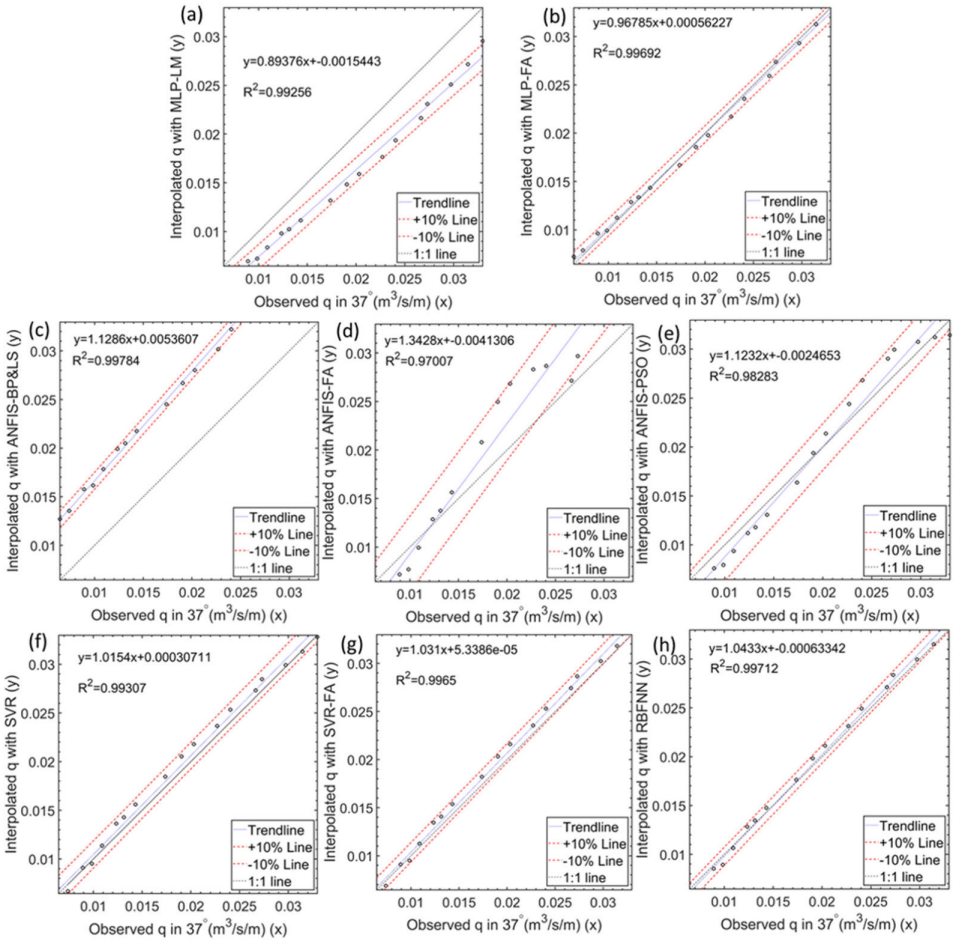

FIGURE 8. Scatter plot for observed q versus estimated q, in the interpolation task (a): MLP-LM (b): MLP-FA (c): ANFIS-BP&LS (d): ANFIS-PSO (e): ANFIS-FA (f): SVR (g): SVR-FA (h): RBFNN.

the interpolation task, which agrees with the reported results in Table 1.

Likewise, distributed points associated with ANFIS-FA and ANFIS-PSO represent an improper fit in Figs. 8(d) and 8(e), respectively. The wider CI in these two SCTs is exposing their imprecise estimation in an intermediate α. However, the higher accuracy of ANFIS-PSO compared to ANFIS-FA is conspicuous in Fig. 8(e).

Figs. 8(f) and 8(g) show that SVR and SVR-FA estimate the q with acceptable accuracy. Moreover, the smaller CI in Fig. 8(g), in comparison with Fig. 8(f), reveals the constructive contribution of using FA in SVR's interpolation accuracy.

The positive influence of FA on SCTs is increasingly apparent in Fig. 8(b) when in comparison with MLP-LM, MLP-FA submits the best fit with the highest correlation and smallest CI. Visual investigation in Figs. 8(b) and 8(h) reveal the uncanny resemblance between MLP-FA and RBFNN performances. It should be noted that without taking advantage of a meta-heuristic training algorithm, RBFNN interpolates the q with considerably high accuracy.

The Taylor diagram is implemented to provide a diagnostic analysis and elucidate the SCTs performance in terms of STD, R, and RMSD. The implemented Taylor diagram for the testing stage and interpolation task is illustrated in Figs. 9(a) and 9(b), respectively.

Fig. 9(a) shows that all the SCTs are accumulated in the area with RMSD less than five, while their distance from the reference point demonstrates their estimation accuracy. Although all the applied SCTs show significant confidence in the testing stage, the applied ANFISs and MLPs have a closer distance from the reference point. In comparison, the ANFIS-PSO is scattered in less distance from the reference point, and MLP-FA takes the second place after it.

As depicted in Fig. 9(b), the superiority of MLP-FA over other applied AI-DMMs in the interpolation task is conspicuous. Moreover, RBFNN could be ranked next after MLP-FA, while SVR-FA and SVR ranked third and fourth, respectively. As stated by the Taylor diagnostic analysis, ANFIS-FA has the most imprecise estimation in the interpolation task. Regarding MLP-LM and ANFIS-PSO, although they are scattered in the area with RMSD less than five,

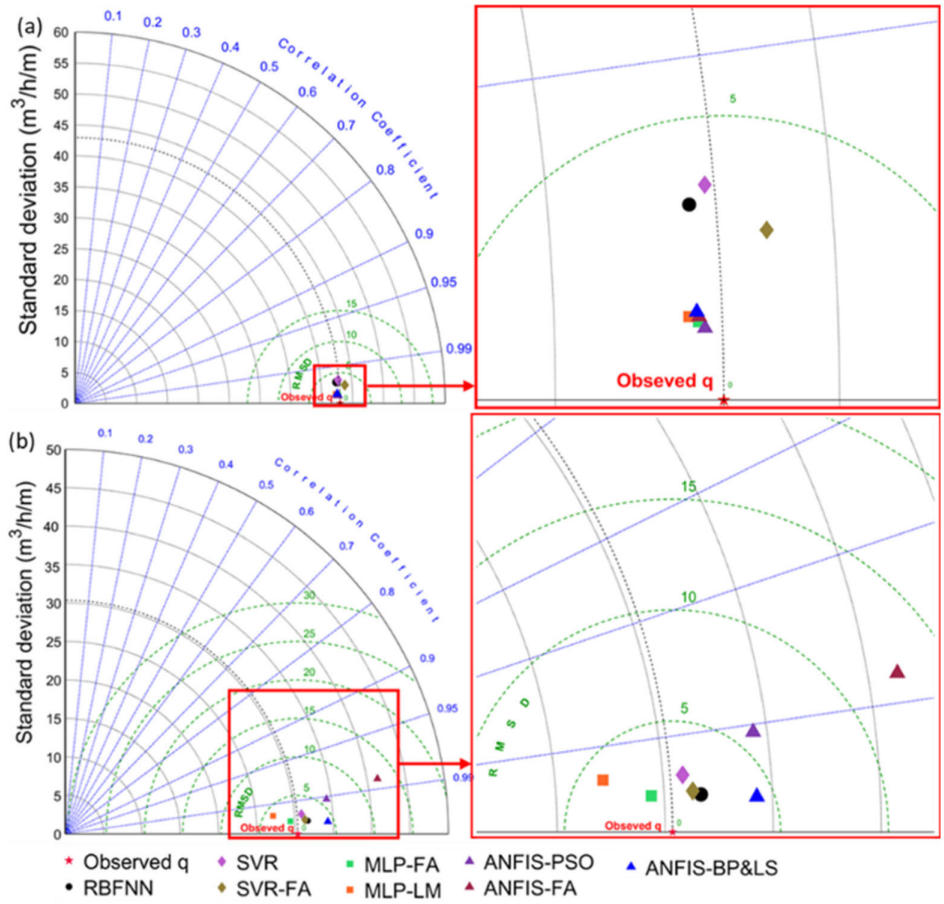

FIGURE 9. Diagnostic analysis using Taylor diagram for all applied SCTs in (a): testing stage (b): interpolation task.

due to their STD, they are scattered far from the reference point.

The results in Table 1, Figs. 6, 7, 8, and 9 indicate the considerable difference between the SCTs' performance in the testing stage and the interpolation task. This difference confirms the study's hypothesis that an SCT's competence in the standard testing approach could not guarantee its accuracy in the interpolation task.

Henceforth, to identify the most accurate SCT for estimating LW's flow rate, the present study systematically investigates the interpolation accuracy of the applied SCTs.

According to Fig. 9(b), ANFIS-PSO and ANFIS-FA estimated the q with lower accuracy than ANFIS-BP&LS, which conflicts with the proposed results in Table 1 and Fig. 8. Hence, besides the Taylor diagram, Kruskal-Wallis and Mann-Whitney tests are implemented to investigate the performance of SCTs in the interpolation task. The results of the Kruskal-Wallis and Mann-Whitney tests are tabulated in Table 3. It should be noted that the implemented Kruskal-Wallis is rejecting the null hypothesis at the 1% significance level with a p-value equivalent to 0.1408, which means at least there is one group with a significant difference from others. Thus, to specify the one or several groups which are different from the observed dataset, a post hoc test is executed, and its results are shown in Fig. 10.

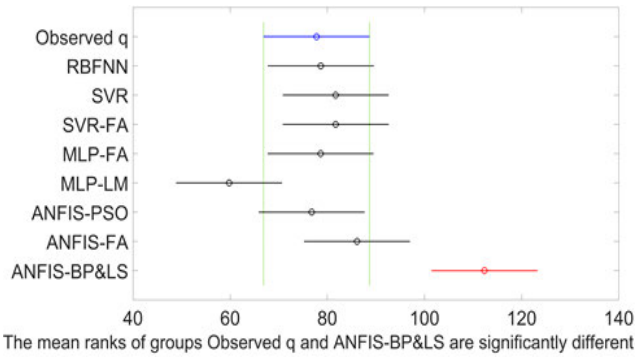

FIGURE 10. implemented post hoc test at the 5% significance level based on the Kruskal-Wallis test's results.

The proposed results in Table 3 for both Kruskal-Wallis and Mann-Whitney tests are in agreement and confirm the superiority of MLP-FA over other applied SCTs in the interpolation task. Similar to the Taylor diagram, RBFNN ranked second. Likewise, SVR and SVR-FA have the same

TABLE 3. The results of Kruskal-Wallis and Mann-Whitney tests between observed and estimated valued in interpolation task.

	Kruskal-Wallis test			Mann-Whitney test		
rank	SCT	Mean rank	Mean rank difference	p-value (SCT vs. Observed q)	significantly different (95%)	significantly different(99%)
0	Observed q in 37°	77.7778	0			
1	MLP-FA	78.6111	0.8333	0.9874	×	×
2	RBFNN	78.6667	0.8889	0.937	×	×
3	ANFIS-PSO	76.7778	-1	0.9118	×	×
4	SVR-FA	81.7222	3.9444	0.8371	×	×
5	SVR	81.7222	3.9444	0.788	×	×
6	ANFIS-FA	86.1111	8.3333	0.6016	×	×
7	MLP-LM	59.7778	-18	0.2232	×	×
8	ANFIS-BP&LS	112.333	34.5555	0.0218	✓	×

TABLE 4. Rankings of the applied SCTs based on their performance in the testing stage and interpolation task.

rank	testing	interpolation
1	ANFIS-PSO	MLP-FA
2	MLP-FA	RBFNN
3	ANFIS-FA	SVR-FA
4	ANFIS-BP&LS	SVR
5	MLP-LM	ANFIS-PSO
6	SVR-FA	MLP-LM
7	SVR	ANFIS-FA
8	RBFNN	ANFIS-BP&LS

mean rank difference in the Kruskal-Wallis test, while the calculated p-value in the Mann-Whitney test for SVR-FA is 0.074 higher than the p-value of SVR.

According to the Taylor diagnostic analysis, ANFIS-FA and ANFIS-PSO have the least accuracy in interpolation tasks, while in Table 3, ANFIS-PSO ranked third, and ANFIS-FA performed better than MLP-LM and ANFIS-BP&LS. Moreover, according to Fig. 10, ANFIS-BP&LS is the only group with a significant difference from the observed data at the 5% significance level. Although the performances of MLP-FA, RBFNN, SVR-FA, and SVR in Table 1, Figs. 7, and 8 agree with the proposed results in Table 3, there are some conflicts about the performances of ANFIS-PSO, ANFIS-FA, ANFIS-BP&LS, and MLP-LM in the mentioned figures and tables. Thus, to clarify these conflicts, H/P versus the interpolated q by each SCT, in addition to the observed q at 37°, are illustrated in Fig. 11.

According to Fig. 11(b), in an intermediate α, MLP-FA, RBFNN, SVR-FA, and SVR estimate q with significant accuracy, confirming that the previous reports and the implemented tests correctly identified their superior performance and appropriately ranked them.

According to Fig. 11(a), ANFIS-BP&LS is capable of estimating the target's trend, which explains the similarity of its STD to the observed value and, subsequently, its higher R in Table 1. These parameters result in better performance of ANFIS-BP&LS in the Taylor diagram. Simultaneously, the considerable difference between estimated q by ANFIS-BP&LS and observed q gives rise to its higher mean rank difference in the Kruskal-Wallis test and smaller p-value

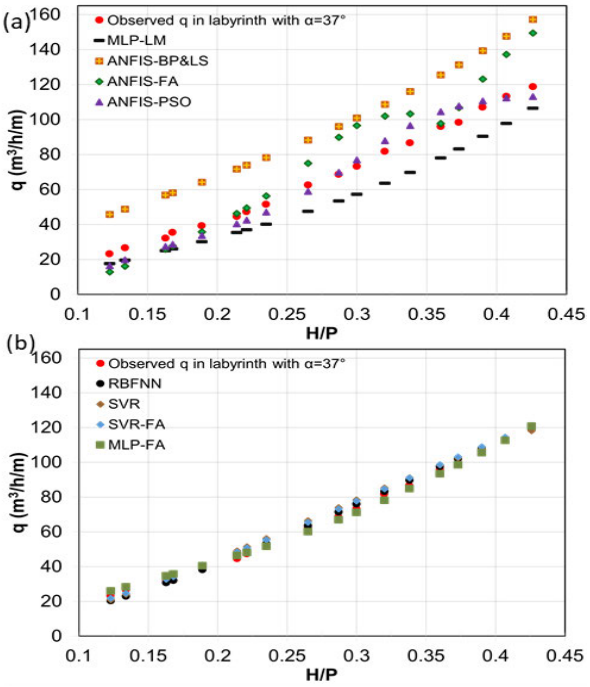

FIGURE 11. (a): the interpolated q by the MLP-LM, ANFIS-BP&LS, ANFIS-FA, and ANFIS-PSO versus H/P (b): the interpolated q by RBFNN, SVR, SVR-FA, MLP-FA RBFNN, SVR, SVR-FA and MLP-FA versus H/P.

in the Mann-Whitney test. Likewise, MLP-LM shows the same behavior with less intensity and in the opposite direction, which is also clearly observable in Figs. 9 and 10. ANFIS-FA is almost incompetent to find the target's trend. Even so, it has notably close estimations to the observed q in five samples. These five precise estimations of ANFIS-FA decrease the mean rank difference in the Kruskal-Wallis test, while the Taylor diagram correctly diagnoses its feeble general performance. Thus, it can be concluded that ANFIS-FA, due to its feeble trending, and ANFIS-BP&LS, due to its high mean rank difference, are the most imprecise methods in the interpolation task.

Visual investigation in Fig. 11(a) reveals that ANFIS-PSO estimates q with higher accuracy than all the other applied ANFISs. However, when H/P is bigger than 0.3,

TABLE 5. Summary reports of the related studies to estimating LW's flow rate using soft computing techniques.

Authors	year	LW configuration	SCT*	Remarks
Emiroglu et al. [14]	2011	Triangular side weirs	ANN	• 2500 data were used to train and test the ANN (60% training) • compared to MNLR and MLR, **ANN** estimated C_d more accurately with 33.28% and 57.79% lower RMSE, respectively.
Kisi et al. [15]	2012	Triangular side weirs	**RBFNN** GRNN GEP	• 2500 data were used to train and test the SCTs (60% training) • **RBFNN** is superior to GRNN and GEP. • In comparison to MNLR, RBFNN reported 35% and 36% lower RMSE and MAE.
Hosseini et al. [16]	2016	Triangular weir	ANFIS	• 34 data were used to train and test the ANFIS (80% training) • **ANFIS** estimated C_d as a function of α and H_t/P • R^2, RMSE, and MAE in the testing stage were equivalent to 0.9988, 0.0087, and 0.00773, respectively.
Zaji et al. [18]	2016	Triangular side weirs	SVR **SVR-FA**	• 200 data were used to train and test the SVRs (50% training) • **SVR-FA** predicted the C_d about 10% more accurate than classic SVR.
Parsaie and Haghiabi [21]	2017	Triangular weir	MLP RBFNN **SVR**	• 223 data were used to train and test the SCTs (80% training) • SVR predicted C_d slightly better than MLP and RBFNN.
Parsaie and Haghiabi [22]	2017	Triangular weir	**MLP** ANFIS SVR GMDH MARS	• 375 data were used to train and test the SCTs (80% training) • MLP predicted C_d whit R^2= 0.9632 and RMSE= 0.077, which was more accurate than SVR, GMDH, ANFIS, MARS, respectively.
Karimi et al. [19]	2017	Triangular weir	**SVR-FA** SVR RSM PCA	• 121 data were used to train and test the SCTs (78% training) • **SVR-FA** reported the most accurate estimation with R^2=0.991, RMSE=0.0035, and MAPE=0.49%
Norouzi et al. [8]	2019	Trapezoidal weir	**MLP** SVR RBFNN	• 454 data were used to train and test the SCTs (75% training) • **MLP** estimated the C_d more accurate compared to SVR and RBFNN
Zounemat and Mahdavi [23]	2020	Piano key weir	MLP MLP-FA MLP-PSO MLP-GA MLP-MFO ANFIS ANFIS-FA **ANFIS -PSO** ANFIS -GA ANFIS -MFO	• 430 data were used to train and test the SCTs (70% training) • **ANFIS-PSO** had the best performance in the testing stage with R^2=0.9998, MSE=1.4 ltr/s, and MAE=1.192 ltr/s • except for ANFIS-MFO, ANFIS structure reported more accurate results in all hybrid meta-heuristic models • In the case of MLP, the FA algorithm could improve the MLP performance more than PSO, GA, and MFO. • MFO leads MLP and ANFIS to unprecise estimations
Shafiei et al. [20]	2020	Triangular weir Trapezoidal weir	ANFIS **ANFIS-FA**	• 470 data were used to train and test the ANFISs (80% training) • **ANFIS-FA** performed more accurate than ANFIS and Computational Fluid Dynamic (CFD)
The Current study		Triangular weir	ANFIS **ANFIS-PSO** ANFIS-FA SVR SVR-FA MLP **MLP-FA** RBFNN	• 206 data were collected from two databases • A novel approach was introduced to assess the SCTs' interpolation accuracy • 151 data used for training, 37 data used for testing, 18 data used to evaluate the SCTs' interpolation accuracy • Hybrid algorithms could improve the performance of the SCTs. • ANFIS-PSO had the best performance in the standard testing approach (similar to the previous studies) • MLP-FA had the most accuracy in the interpolation task • In LW's discharge estimation, the competence of an SCT in the standard testing approach could not guarantee its accuracy in estimating intermediate values which are not similar to either testing or training data

*note: **ANN**: Artificial Neural Network; **RBFNN**: Radial Basis Function Neural Network; **GRNN**: General Regression Neural Network; **GEP**: Gene-Expression Programming; **ANFIS**: Adaptive Neuro-Fuzzy Inference System; **PSO**: Particle Swarm Optimization; **SVR**: Support Vector Regression; **FA**: Firefly optimization Algorithm; **MLP**: Multi-Layer Perceptron; **GMDH**: Group Method of Data Handling; **MARS**: Multivariate Adaptive Regression Splines; **RSM**: Response Surface Methodology; **PCA**: Principal Component Analysis; **GP**: Genetic Programming; **GA**: Genetic Algorithm; **MFO**: Moth-Flame Optimization

ANFIS-PSO slightly loses the target's trend, which causes lower R, higher STD, and RMSD. Thus, in the Taylor diagram (Fig. 9(b)), ANFIS-PSO is assigned to a location even inferior to ANFIS-BP&LS. However, the small difference between the observed q and interpolated q by ANFIS-PSO results in better performance in the Kruskal-Wallis test. Thereby, it can be concluded that, although ANFIS-PSO is more accurate than MLP-LM, ANFIS-BP&LS, and ANFIS-FA, its performance is inferior to SVR and SVR-FA. Eventually, as the final result, the present research offerings Table 4. This table comprises two rankings for the applied SCTs, based on their performance in the testing stage and interpolation task.

According to Table 4, it is being suggested that for predicting/forecasting/estimating data with no intermediate values (e.g., forecasting time-series), the SCT be chosen based on its rank in the testing stage. In contrast, for estimating/predicting data with intermediate values (e.g., discharge capacity or discharge coefficient in an LW), it is being recommended to select an SCT based on its rank in the interpolation task.

In order to have a better insight and an overall judgment for the applied methodology, the previous studies' outcomes have been considered, and the general remarks are presented in Table 5.

Table 5 indicates that the compared SCTs in this research are the most accurate techniques reported in similar studies to this paper's topic. It is noticeable that these techniques were not compared with each other previously, particularly in terms of interpolation accuracy.

IV. CONCLUSION

Soft Computing Techniques (SCT) are extensively used to estimate Labyrinth Weir's (LW) flow-rate. Due to the multiplicity of the employed SCTs, identifying the most competent SCT is indispensable. The present study exploited the four most accurate techniques, including ANFIS, MLP, SVR, and RBFNN, to estimate discharge per unit width (q) of a sharp-crest triangular LW in the free-flow condition. Additionally, two popular meta-heuristic algorithms (i.e., PSO and FA) were joined with these techniques and provided four hybrid techniques, including MLP-FA, ANFIS-PSO, ANFIS-FA, and SVR-FA. It can be stated that no published literature evaluates these SCTs simultaneously.

Although there are numerous experimental studies on LW, all of them were conducted for some limited LW's side angles (α). Thus, all the proposed empirical models can only estimate the flow-rate or discharge coefficient in those experimented α angles. Nonetheless, in real-world problems, LW is being designed with an α not precisely equal to the experimented angles. Furthermore, in previous studies wherein researchers have employed SCTs to estimate the LW's flow rate, their applied SCTs have been evaluated with a random testing dataset (i.e., standard testing approach). Thus, despite the importance of SCT's interpolation accuracy, it was not investigated previously.

In order to investigate the SCTs' interpolation accuracy, the current study defined a hypothesis that the competence of an SCT in the standard testing approach could not guarantee its accuracy in estimating intermediate data that are not similar to either testing or training data. Therefore, in addition to the standard testing approach, a novel approach for assessing the SCTs' interpolation accuracy was proposed. To this end, one set of data with an intermediate α was excluded from the training and testing dataset. Afterward, the trained SCTs were used to estimate the discharge in the excluded α.

The general evaluation based on several statistical criteria (R, IA, NSE, MAE, RMSE, MAPE) indicated that all the applied SCTs estimate the q more accurately than empirical models. Correspondingly, ANFIS-PSO (R = 0.9996, MAPE = 2.103%) submitted the best performance in the standard testing approach. Comparing the obtained results in the standard testing approach with the most accurate SCTs have been reported in the previous studies implied the superiority of ANFIS-PSO.

Regarding the novel approach proposed for assessing the SCTs' interpolation accuracy, it was concluded that the competence of an SCT in the testing stage could not guarantee its accuracy in the interpolation task. Subsequently, in contrast with the testing stage, wherein ANFIS-PSO was superior, MLP-FA (R = 0.9984, MAPE = 3.284%) had the best fit in the interpolation task. In order to ensure the study's hypothesis, the outcomes of SCTs were evaluated through scatter plots, the Taylor diagnostic test, Kruskal-Wallis, and Mann-Whitney tests. The implemented tests confirmed the constructive contribution of PSO and FA in training SCTs, while magnified the considerable difference between STCs performance in the testing stage and interpolation task.

The employed Kruskal-Wallis test revealed that at least the outcome of one SCTs in the interpolation task has a significant difference with others at 1%. Thereupon, the applied post hoc test at the 5% significant level based on Kruskal-Wallis test results showed that in the interpolation task, the results of ANFIS-BP&LS has a significant difference with the observed data. Likewise, the Mann-Whitney test confirmed that except for ANFIS-BP&LS, there is no significant difference between observed data and estimated data in the interpolation task at 99%.

According to the reported results, RBFNN, SVR, and SVR-FA did not submit the highest accuracy in the testing and interpolation stages. Nonetheless, their average performance in both testing and interpolation stages was acceptable, which cannot be stated for ANFISs and MLPs.

Concerning the proposed results, implemented tests, and visual investigation in outcomes of SCTs, two rankings were offered for all the applied SCTs based on their performance in the testing stage and interpolation task.

REFERENCES

[1] J. P. Tullis, N. Amanian, and D. Waldron, "Design of labyrinth spillways," *J. Hydraulic Eng.*, vol. 121, no. 3, pp. 247–255, Mar. 1995.
[2] B. M. Crookston, "Labyrinth weirs," Ph.D. dissertation, Dept. Civil Environ. Eng., Utah State Univ., Logan, UT, USA, 2010. [Online]. Available: https://digitalcommons.usu.edu/etd/802
[3] G. Taylor, "The performance of labyrinth weirs," Ph.D. dissertation, Dept. Appl. Sci., Univ. Nottingham, Nottingham, U.K., 1968. [Online]. Available: https://core.ac.uk/download/pdf/33565801.pdf
[4] M. C. Aydin and M. E. Emiroglu, "Determination of capacity of labyrinth side weir by CFD," *Flow Meas. Instrum.*, vol. 29, pp. 1–8, Mar. 2013.
[5] B. M. Crookston and B. P. Tullis, "Hydraulic design and analysis of labyrinth weirs. I: Discharge relationships," *J. Irrig. Drain. Eng.*, vol. 139, no. 5, pp. 363–370, May 2013.
[6] S. Kumar, Z. Ahmad, and T. Mansoor, "A new approach to improve the discharging capacity of sharp-crested triangular plan form weirs," *Flow Meas. Instrum.*, vol. 22, no. 3, pp. 175–180, Jun. 2011.
[7] M. Bijankhan and S. Kouchakzadeh, "Unified discharge coefficient formula for free and submerged triangular labyrinth weirs," *Flow Meas. Instrum.*, vol. 57, pp. 46–56, Oct. 2017.
[8] R. Norouzi, R. Daneshfaraz, and A. Ghaderi, "Investigation of discharge coefficient of trapezoidal labyrinth weirs using artificial neural networks and support vector machines," *Appl. Water Sci.*, vol. 9, no. 7, pp. 1–10, Oct. 2019.

[9] B. M. Crookston and B. P. Tullis, "Labyrinth weirs: Nappe interference and local submergence," *J. Irrigation Drainage Eng.*, vol. 138, no. 8, pp. 757–765, Aug. 2012.

[10] B. Gentilini, "Stramazzi con cresta a planta obliqua e a zig-zag," *Mem. e Stud. dell Inst. di Idraul. e Construzioni Idraul. del Regil Politec. di Milano*, vol. 48, no. 16, Oct. 1940. [Online]. Available: https://books.google.com.tw/books?id=J23SAAAAMAAJ&printsec=frontcover#v=onepage&q&f=false

[11] B. P. Tullis, J. C. Young, and M. A. Chandler, "Head-discharge relationships for submerged labyrinth weirs," *J. Hydraulic Eng.*, vol. 133, no. 3, pp. 248–254, Mar. 2007.

[12] M. Ghodsian, "Stage–discharge relationship for a triangular labyrinth spillway," *Proc. Inst. Civil Eng. Water Manag.*, vol. 162, no. 3, pp. 173–178, 2009.

[13] R. Lopes, J. Matos, and J. F. de Melo, "Discharge capacity and residual energy of labyrinth weirs," in *Proc. Int. Junior Res. Eng. Workshop Hydraulic Struct.*, J. Matos and H. Chanson, Eds., 2006, pp. 47–56.

[14] M. E. Emiroglu, O. Bilhan, and O. Kisi, "Neural networks for estimation of discharge capacity of triangular labyrinth side-weir located on a straight channel," *Expert Syst. Appl.*, vol. 38, no. 1, pp. 867–874, Jan. 2011.

[15] O. Kisi, M. Emin Emiroglu, O. Bilhan, and A. Guven, "Prediction of lateral outflow over triangular labyrinth side weirs under subcritical conditions using soft computing approaches," *Expert Syst. Appl.*, vol. 39, no. 3, pp. 3454–3460, Feb. 2012.

[16] K. Hosseini, E. J. Nodoushan, R. Barati, and H. Shahheydari, "Optimal design of labyrinth spillways using meta-heuristic algorithms," *KSCE J. Civil Eng.*, vol. 20, no. 1, pp. 468–477, Jan. 2016.

[17] A. Hossein Zaji, H. Bonakdari, and S. Karimi, "Radial basis neural network and particle swarm optimization-based equations for predicting the discharge capacity of triangular labyrinth weirs," *Flow Meas. Instrum.*, vol. 45, pp. 341–347, Oct. 2015.

[18] A. H. Zaji, H. Bonakdari, S. R. Khodashenas, and S. Shamshirband, "Firefly optimization algorithm effect on support vector regression prediction improvement of a modified labyrinth side weir's discharge coefficient," *Appl. Math. Comput.*, vol. 274, pp. 14–19, Feb. 2016.

[19] H. Karami, S. Karimi, M. Rahmanimanesh, and S. Farzin, "Predicting discharge coefficient of triangular labyrinth weir using support vector regression, support vector regression-firefly, response surface methodology and principal component analysis," *Flow Meas. Instrum.*, vol. 55, pp. 75–81, Jun. 2017.

[20] S. Shafiei, M. Najarchi, and S. Shabanlou, "A novel approach using CFD and neuro-fuzzy-firefly algorithm in predicting labyrinth weir discharge coefficient," *J. Brazilian Soc. Mech. Sci. Eng.*, vol. 42, no. 1, pp. 1–19, Jan. 2020.

[21] A. Parsaie and A. H. Haghiabi, "Support vector machine to predict the discharge coefficient of sharp crested W-planform weirs," *AUT J. Civil Eng.*, vol. 1, no. 2, pp. 195–204, 2017.

[22] A. Parsaie and A. H. Haghiabi, "Improving modelling of discharge coefficient of triangular labyrinth lateral weirs using SVM, GMDH and MARS techniques," *Irrigation Drainage*, vol. 66, no. 4, pp. 636–654, Oct. 2017.

[23] M. Zounemat-Kermani and A. Mahdavi-Meymand, "Hybrid meta-heuristics artificial intelligence models in simulating discharge passing the piano key weirs," *J. Hydrol.*, vol. 569, pp. 12–21, Feb. 2019.

[24] L. Penghui, A. A. Ewees, B. H. Beyaztas, C. Qi, S. Q. Salih, N. Al-Ansari, S. K. Bhagat, Z. M. Yaseen, and V. P. Singh, "Metaheuristic optimization algorithms hybridized with artificial intelligence model for soil temperature prediction: Novel model," *IEEE Access*, vol. 8, pp. 51884–51904, 2020.

[25] J. Kennedy, R. C. Eberhart, and Y. Shi, *Swarm Intelligence*. San Mateo, CA, USA: Morgan Kaufmann Publishers, 2001.

[26] X. S. Yang, "Firefly algorithms for multimodal optimization," in *Proc. Int. Symp. Stochastic Algorithms*, in Lecture Notes in Computer Science, vol. 5792, 2009, pp. 169–178.

[27] B. Chopard and M. Tomassini, *An Introduction to Metaheuristics for Optimization*. Cham, Switzerland: Springer, 2018.

[28] S. Haykin, *Neural Networks and Learning*, 3rd ed. Hamilton, ON, Canada: Pearson, 2009.

[29] D. S. Broomhead and D. Lowe, "Multivariable functional interpolation and adaptive networks," *Complex Syst.*, vol. 2, no. 3, pp. 321–355, 1988.

[30] M. Amirian and F. Schwenker, "Radial basis function networks for convolutional neural networks to learn similarity distance metric and improve interpretability," *IEEE Access*, vol. 8, pp. 123087–123097, 2020.

[31] I. Aleksander and H. Morton, *An Introduction to Neural Computing*. London, U.K.: Chapman & Hall, 1990.

[32] R. Kruse, C. Borgelt, F. Klawonn, C. Moewes, M. Steinbrecher, and P. Held, "Radial basis function networks," in *Computational Intelligence*, vol. 56, no. 7/2008. London, U.K.: Springer, 2013, ch. 6, pp. 83–103. [Online]. Available: http://link.springer.com/10.1007/978-1-4471-5013-8

[33] V. Vapnik, *The Nature of Statistical Learning Theory*. New York, NY, USA: Springer, 1995.

[34] W. Cao, X. Liu, and J. Ni, "Parameter optimization of support vector regression using Henry gas solubility optimization algorithm," *IEEE Access*, vol. 8, pp. 88633–88642, 2020.

[35] J.-S. R. Jang, "ANFIS: Adaptive-network-based fuzzy inference system," *IEEE Trans. Syst., Man, Cybern.*, vol. 23, no. 3, pp. 665–685, Jun. 1993.

[36] S. L. Chiu, "Fuzzy model identification based on cluster estimation," *J. Intell. Fuzzy Syst.*, vol. 2, no. 3, pp. 267–278, 1994.

[37] K. E. Taylor, "Summarizing multiple aspects of model performance in a single diagram," *J. Geophys. Res., Atmos.*, vol. 106, no. D7, pp. 7183–7192, Apr. 2001.

[38] W. H. Kruskal and W. A. Wallis, "Use of ranks in one-criterion variance analysis," *J. Amer. Stat. Assoc.*, vol. 47, no. 260, pp. 583–621, Dec. 1952.

[39] K. L. Houston, "Hydraulic model study of Ute dam labyrinth spillway," BRERC, Denver, CO, USA, Tech. Rep., Aug. 1982. [Online]. Available: https://www.usbr.gov/tsc/techreferences/research/GR-82-07.pdf

[40] H. M. Azamathulla, S. Emamgholizadeh, A. Parsaie, and A. H. Haghiabi, "Prediction of discharge coefficient of combined weir-gate using ANN, ANFIS and SVM," *Int. J. Hydrol. Sci. Technol.*, vol. 9, no. 4, p. 412, 2019.

[41] S. A. Kalogiro and M. Bojic, "Artificial neural networks for the prediction of the energy consumption of a passive solar building," *Energy*, vol. 25, no. 5, pp. 479–491, 2000.

ALI MAHMOUD received the master's degree in hydraulic structure, in 2014. He is currently pursuing the Ph.D. degree with the School of Civil and Hydraulic Engineering, Huazhong University of Science and Technology. He won the Chinese Government Scholarship, in 2017. His research interests include soft computing techniques, evolutionary computation, modeling and simulation, multi-objective optimization, and applications in hydraulic structures, dams, and spillways.

XIAOHUI YUAN (Senior Member, IEEE) received the Ph.D. degree in hydropower engineering from the Huazhong University of Science and Technology, China, in 2002. He is currently a Professor with the School of Hydropower and Information Engineering, Huazhong University of Science and Technology. His research interests include evolutionary computation, complex system modeling and simulation, system optimization and its applications.

MARWAN KHEIMI received the Ph.D. degree in civil engineering and water resources from the University of Central Florida, Orlando, FL, USA, in 2019. He is currently a Faculty Member with the Department of Civil and Environment Engineering, Faculty of Engineering, Rabigh, Saudi Arabia. His research interests include hydrological, watershed, water balance modeling, GIS and remote sensing applications, and optimization models.

YANBIN YUAN received the Ph.D. degree in geodetection and information technology from the China University of Geosciences, Wuhan, in 2000. He is currently a Professor of Information System with the Wuhan University of Technology, China. His research interests include mineral resource prospecting and exploration, geographical information systems, hydrology, and water resources. He is a member of IAMG and GSC.